

Suppression of long-time anomalies in simple classical liquids

J. Bosse, W. Götze, and M. Lücke

Max-Planck-Institut für Physik und Astrophysik, D-8000 München, Germany
and Physik Department der Technischen Universität München, 8046 Garching, Germany

(Received 15 May 1979)

The spectrum of the velocity-autocorrelation function at small frequencies is evaluated within mode-coupling theory for liquid argon at the triple point and for liquid rubidium. We investigate the dynamical processes limiting the asymptotic range over which the low-frequency square-root cusp of the spectrum can be observed. The frequency dependence of the shear viscosity is shown to have the largest effect upon the suppression of the anomalous long-time decay of velocity correlations. Our results indicate that in the high-density fluids considered the above anomaly shows up only as a percent contribution to the spectrum below some 10^{11} sec⁻¹.

The long-time anomaly of correlation functions has stimulated research activities¹ ever since the discovery² of the nonexponential decay $t^{-3/2}$ of the velocity-autocorrelation function (VAF)

$$\psi(t) = \frac{1}{3} \langle \vec{v}(t) \cdot \vec{v} \rangle \quad (1)$$

of a tagged hard sphere moving in a hard-sphere fluid. The above power-law tail of $\psi(t)$ can be explained^{3,4} in a hydrodynamic picture by long-living shear excitations generated by the motion of the considered particle. The shear excitations diffuse into the fluid previously at rest such that the radius $R(t)$ of the flow pattern surrounding the particle grows proportional to $\sqrt{D_T t}$, where D_T denotes the kinematic viscosity. Momentum conservation then forces the particle's velocity to decrease as $R^{-3}(t)$.

To take into account the fluctuations which were neglected in the above explanation kinetic equations including repeated collisions⁵ and mode-coupling approximations¹ have been investigated. Both approaches give for the long-time decay of the VAF

$$\psi(t \rightarrow \infty) = (T/12nm) [\pi(D + D_T)t]^{-3/2}, \quad (2)$$

with T denoting the temperature ($k_B = 1$) and n the particle number density of the fluid, m being the particle's mass, and D the self-diffusion coefficient. The spectrum

$$\psi''(\omega) = \frac{1}{2T} \int_{-\infty}^{\infty} dt e^{i\omega t} \psi(t) \quad (3)$$

of the VAF (1) shows a low-frequency square-root cusp due to (2)

$$\psi''(\omega \rightarrow 0) = (D/T) [1 - (\omega/\omega_0)^{1/2} + \dots], \quad (4)$$

The inverse of the frequency

$$\omega_0 = 72(\pi nm D/T)^2 (D + D_T)^3 \quad (5)$$

measures the steepness of the square-root decrease (4).

The cusp (4) is superimposed on a broad spectral background of $\psi''(\omega)$ which increases with frequen-

cy in dense fluids such as Ar close to its triple point as a consequence of strong correlation effects.⁶ That implies a minimum in the spectrum $\psi''(\omega)$ at a frequency ω_{\min} below which the anomalous low-frequency asymptotics (4) can be seen and above which the increase of the background dominates. The relevant question pertaining to an experimental verification of (4) is how large is the frequency of the minimum, or equivalently, what is the time ω_{\min}^{-1} above which the long-time tail is observable. Having determined ω_{\min} , one obtains in addition a quantitative expression for the relative strength of the low-frequency cusp caused by the long-time tail of the VAF

$$\sigma = \frac{\psi''(0) - \psi''(\omega_{\min})}{\psi''(0)} \approx \left(\frac{\omega_{\min}}{\omega_0} \right)^{1/2}. \quad (6)$$

At present there is little experimental information available regarding the cusp (4). Rahman⁷ did not find it in his computer simulation for $\psi''(\omega)$ of liquid argon at the triple point. A value of $\omega_{\min} \approx 0.6 \times 10^{11}$ s⁻¹ was found by Levesque and Ashurst⁸ in a molecular-dynamics (MD) experiment involving 4000 particles which interact via a soft repulsive potential provided argon parameters are used to determine the frequency scale. However, the simulation was performed at one-half the density and three times the temperature of the argon triple point. Michels and Trappeniers⁹ investigated Lennard-Jones systems at various densities and temperatures well away from the triple point of argon. For their largest density ($\frac{1}{3}n_{\text{triple}}$) and lowest temperature ($2T_{\text{triple}}$) they report a $t^{-3/2}$ tail for times larger than 8.5×10^{-12} s.

$\psi''(\omega)$ can be extracted from the zero-wave-number limit of the incoherent Van Hove function $S_s(q, \omega)$ (Ref. 10) and so, in principle, it can be measured by inelastic-neutron-scattering experiments. Carneiro¹¹ analyzed the data for $S_s(q, \omega)$ of Sköld *et al.*¹² and concluded that $\sigma(6)$ could be as large as 0.38. The extrapolation¹¹ from the large

wave numbers probed by neutrons down to $q=0$ implies, of course, considerable uncertainties.

Here we want to clarify the question concerning the size of σ somewhat more quantitatively. Furthermore, the physical reason for ω_{\min} being as small as 10^{11} s^{-1} will be investigated at length. Both are done within the framework of the self-consistent mode-coupling theory for the excitation spectra of liquid argon and rubidium.¹³⁻¹⁵ The results for the spectra of the VAF (Ref. 15) do not display a low-frequency spike (4) and hence the frequency resolution $\Delta\omega = 5 \times 10^{11} \text{ s}^{-1}$ employed in the above calculation¹⁵ gives for ω_{\min} as well as for σ an upper bound consistent with the molecular-dynamics experiments. So let us proceed towards a more detailed investigation of $\psi''(\omega)$ for small frequencies.

We will use the representation¹⁵

$$\psi''(\omega) = \frac{\Omega_E^2}{m} \frac{M''(\omega)}{[\omega^2 - \Omega_E^2 + \omega M'(\omega)]^2 + [\omega M''(\omega)]^2} \quad (7)$$

in terms of the real and imaginary part of the complex relaxation kernel

$$M(\omega + i0) = M'(\omega) + iM''(\omega) \quad (8)$$

and the Einstein frequency Ω_E (Ref. 10) of the liquid. Since $M''(\omega)$ is even and $M'(\omega)$ is odd in ω the low-frequency behavior of $\psi''(\omega)$ [Eq. (7)] is determined by that one of the kernel $M''(\omega)$

$$\psi''(\omega \rightarrow 0)/\psi''(0) = M''(\omega \rightarrow 0)/M''(0). \quad (9)$$

For the spectrum of the relaxation kernel the mode-coupling approximation

$$M''(\omega) = M_L''(\omega) + 2M_T''(\omega), \quad (10a)$$

$$M_{L,T}''(\omega) = \frac{\Omega_E^2}{6\pi^2 n} \int_0^\infty dk k^2 V_{L,T}^2(k) \times \int_{-\infty}^\infty \frac{d\epsilon}{\pi} \phi_0''(k, \epsilon) \phi_{L,T}''(k, \omega - \epsilon) \quad (10b)$$

has been derived.¹⁵ The decay vertices approach unity for small wave numbers like $V_{L,T}(k) = 1 - O(k^2)$. They couple via the relaxation-kernel velocity fluctuations of the tagged particle to two-mode excitations described by the convolution (10b) of the incoherent density excitation spectrum $\phi_0''(q, \omega) = \pi S_s(q, \omega)$ with the relaxation spectrum $\phi_{L,T}''(q, \omega)$ of the coherent longitudinal and transverse current fluctuations. The above set of equations (7), (8), and (10) ensures the exact short-time behavior of the VAF

$$\psi(t \rightarrow 0) = (T/m) [1 - \frac{1}{2}(\Omega_E t)^2 + O(t^4)] \quad (11)$$

as well as the correct long-time asymptotics (2).

The regular contributions to $M''(\omega)$ (10) from nonhydrodynamic wave numbers and frequencies larger than the resolution accuracy employed in

Ref. 15 have been represented there. Here we will investigate those contributions to the low-frequency relaxation kernel stemming from wave numbers smaller than $k_0 = 0.1q_0$, where q_0 denotes the main-peak position of the static structure factor. This cutoff was chosen such that for the contributions to (10b) from $k < k_0$: (i) the vertices are practically unity; (ii) the longitudinal propagators can be replaced by the hydrodynamic ones

$$\phi_0(k, \omega + i0) = -1/(\omega + ik^2D), \quad (12)$$

$$\phi_L(k, \omega + i0) = -\omega/(\omega^2 - c^2k^2 + ik^2\omega D_L); \quad (13)$$

(iii) the transverse propagator

$$\phi_T(k, \omega + i0) = -1/[\omega + k^2D_T(\omega + i0)] \quad (14a)$$

contains nonhydrodynamic corrections only via the frequency dependence of the kinematic viscosity

$$D_T(\omega + i0) = iD_T \left(\delta_T + (1 - \delta_T) \frac{i\Gamma_T}{\omega + i\Gamma_T} \right). \quad (14b)$$

Since $M_L''(\omega)$ reflects the coupling of the particle's velocity fluctuation to (propagating) density excitations which rapidly carry away the particle's momentum, $M_L''(\omega)$ does not contribute to the long-time tail. Hence, it is sufficient to use the hydrodynamic propagator (13) when studying the influence of the background contribution $M_L''(\omega)$ upon the size of ω_{\min} . Also, in $\phi_0(k, \omega + i0)$ [Eq. (12)] one does not have to consider frequency- or wave-number-dependent corrections to the transport coeffi-

TABLE I. Parameters for Ar and Rb.

	Argon	Rubidium
$T/^\circ\text{K}$	85	319
$n/\text{\AA}^{-3}$	0.0214	0.010 58
$m/10^{-24} \text{ g}$	66	142
$\Omega_E/10^{13} \text{ s}^{-1}$	0.78	0.61
$v_{\text{th}}/10^5 \text{ cm s}^{-1}$	0.1333	0.1761
$c/10^5 \text{ cm s}^{-1}$	0.595	1.137
$D_L/10^{-3} \text{ cm}^2 \text{ s}^{-1}$	23.2	11.7
$D/10^{-3} \text{ cm}^2 \text{ s}^{-1}$	0.022	0.021
$D_T/10^{-3} \text{ cm}^2 \text{ s}^{-1}$	4.89	5.19
δ_T	0.145	0.140
$\Gamma_T/10^{13} \text{ s}^{-1}$	0.05	0.05
$q_0/\text{\AA}^{-1}$	2	1.54
k_0/q_0	0.1	0.1
$\omega_0/10^{13} \text{ s}^{-1}$	59.1	5.2
$\alpha_L = D_L/D$	1055	557
$\alpha_T = \delta_T D_T/D$	32	35
$\beta_L = (ck_0/Dk_0^2)^2$	1.83×10^4	12.4×10^4
$\beta_T = (D_T/D)(\Gamma_T/Dk_0^2)$	1.26×10^4	2.48×10^4
$\gamma_L = 0$	0	0
$\gamma_T = \Gamma_T/Dk_0^2$	57	100
$M''(\omega=0)^H/\Omega_E$	4.7882×10^{-2}	5.7733×10^{-2}

cient. They would not show up in the convolution integral (10b) since $D \ll D_T$ (cf. Table I). However, the frequency dependence of the kinematic viscosity $D_T(\omega + i0)$ is crucial in explaining the strength σ of the low-frequency anomaly.

For the present purpose the simple parametrization (14b) for $D_T(\omega + i0)$ is sufficient to describe the characteristic two-time structure of $D_T(t)$ found in MD experiments¹⁶ and within the mode-coupling approach.¹⁴ Furthermore, (14b) still allows for an analytical evaluation of the mode-coupling integral (10b).

Inserting in (10b) for the absorptive parts $\phi''(k, \omega)$ of the relaxation functions [Eqs. (12)–(14)] $\text{Im}\phi(k, \omega + i0)$, one can perform the frequency integration in (10b) by the calculus of residues. Although extending to $|\epsilon| = \infty$, the above frequency integral sums effectively only hydrodynamic contributions since, with $k < k_0$, the propagators (12)–(14) rapidly vanish for large frequencies. The remaining wave-number integral up to k_0 over the residues is elementary and yields

$$\frac{M''_{L,T}(\omega)^H}{\Omega_E} = \frac{\Omega_E}{k_0^2 D} \frac{\frac{1}{3} k_0^3 4\pi}{n(2\pi)^3} \frac{1}{\alpha + 1} \times \left\{ 1 + \text{Im} \left[\frac{\hat{\omega} + i\gamma + iA_+ \sqrt{A_+}}{A_+ - A_-} \right] \times \ln \left(\frac{\sqrt{A_+} - 1}{\sqrt{A_+} + 1} \right) + (A_+ \leftrightarrow A_-) \right\}, \quad (15a)$$

where A_{\pm} denote the roots of the quadratic equation

$$A^2 - \left(i \frac{\alpha + 2}{\alpha + 1} \hat{\omega} - \frac{\beta + \gamma}{\alpha + 1} \right) A - \frac{\hat{\omega}^2 + i\hat{\omega}\gamma}{\alpha + 1} = 0 \quad (15b)$$

and $\hat{\omega} = \omega / (k_0^2 D)$. The definitions of the parameters $\alpha_{L,T}$, $\beta_{L,T}$, and $\gamma_{L,T}$ can be found together with their values in Table I. The superscript H reminds that (15) represents only the small-wave-number contributions from the hydrodynamic propagators (12)–(14) to $M''(\omega)$ [Eq. (10b)]. Since D is much smaller than $D_{T,L}$ the expression (15) is very well approximated by its somewhat simpler asymptotic form for $D \rightarrow 0$ ($\beta \rightarrow \infty$) which can also be derived directly from (10b) with $\phi''_0(\omega) \approx \pi \delta(\omega)$.

The full curves in Fig. 1 show

$$M''(\omega)^H = M''_L(\omega)^H + 2M''_T(\omega)^H$$

obtained from Eqs. (15) with the parameters $D_{L,T}$, δ_T , Γ_T , and D (cf. Table I) resulting from the mode-coupling calculations^{14,15} for Ar and Rb. For the sake of comparison the well-known low-frequency asymptotes leading to (4) via relation (9) is given by the dashed curves.

One can distinguish three different effects which

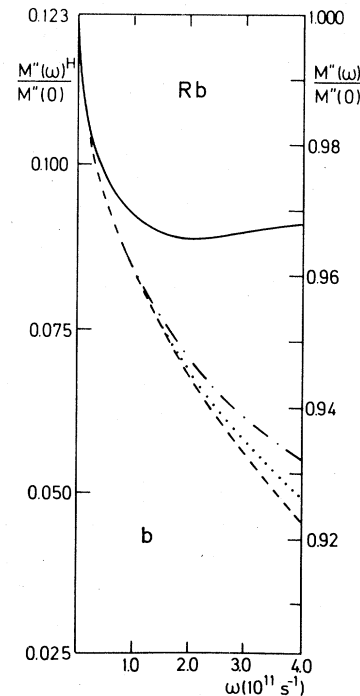
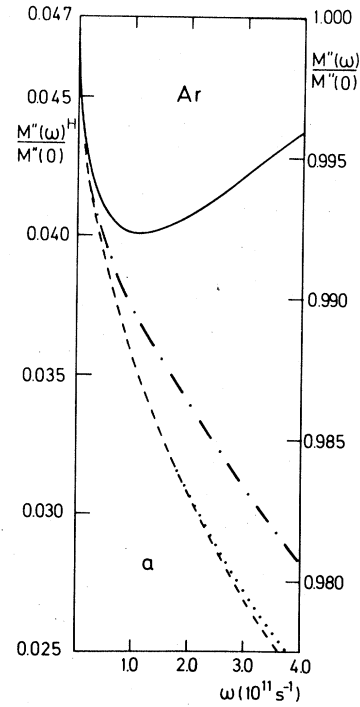


FIG. 1. Low-frequency spectra of the relaxation kernel $M''(\omega)^H$ [Eq. (15)] (full line) for Ar (a) and Rb (b). Dash-dotted curve: $M''(\omega)^H$ obtained with a frequency-independent viscosity ($\delta_T=1$). Dotted curve: only transverse contribution with $\delta_T=1$. Dashed curve: $\omega^{1/2}$ asymptote [Eqs. (4) and (9)]. For further information consult the text.

weaken the low-frequency anomaly: The first one, being numerically irrelevant, reflects higher-order corrections to the square-root behavior. They explain the difference between the dashed and the dotted curves the latter denoting $2M_T''(\omega)^H$ obtained with $\delta_T = 1$ in (14b), i.e., with a purely hydrodynamical transverse propagator (14a).

Adding the longitudinal contribution $M_L''(\omega)^H$ [Eq. (15)] to the dotted curves results in the dash-dotted curves which thus display the effect of the coupling of the tagged particle to the propagating, longitudinal, hydrodynamical bath modes. The comparison of the dotted with the dash-dotted curves shows that this coupling increases monotonously. This effect broadens the low-frequency spikes in $M''(\omega)$ and $\psi''(\omega)$ and it furthermore causes¹⁵ the increase of $\psi''(\omega)$ for larger frequencies. The additional coupling to the longitudinal modes would give rise to a shallow minimum of $\psi''(\omega)$ at a frequency outside the range investigated here.

The third effect, $\delta_T < 1$, suppresses the actual long-time tail even more. The full curves show that taking into account the frequency dependence of the kinematic viscosity $D_T''(\omega)$ [Eq. (14b)] has the largest influence upon the long-time tail. Since $D_T''(\omega)$ [Eq. (14b)] quickly drops to the plateau value δ_T with increasing frequency, the spectra $M''(\omega)$ and $\psi''(\omega)$ soon deviate from the initial $\omega^{1/2}$ decrease and show an increase. This leads together with the other effects to a minimum in $M''(\omega)$ and $\psi''(\omega)$ at a rather small frequency $\omega_{\min} \approx 10^{11} \text{ s}^{-1}$ for Ar and $\omega_{\min} \approx 2 \times 10^{11} \text{ s}^{-1}$ for Rb as shown in Figs. 1 and 2. With the parameters listed in Table I one then obtains only a strength of $\sigma \approx 0.01$ (0.04) for the long-time singularity of Ar (Rb).

So one concludes: Above all it is the pronounced frequency variation of the kinematic viscosity $D_T''(\omega)$ [Eq. (14b)] explained to be due to mode-decay kinematics¹⁴ which suppresses the long-time singularity. The steeper the decrease of $D_T''(\omega)$ with increasing frequency, the larger the time above which the $t^{-3/2}$ decay dominates $\psi(t)$. The hydrodynamical picture of Alder and Wainwright^{3,4} has thus to be supplemented by including the "viscoelastic" effects reflected by the frequency-dependent viscosity. They allow propagation of shear faster than purely hydrodynamical diffusion so that $R(t)$ grows faster than with \sqrt{t} . Since Rb and also Ar behave somewhat like a solid, it takes a very long time before transverse momentum propagates by pure diffusion.

That also explains why it is easier to discover a long-time tail of the VAF in a hard-sphere fluid rather than in a real liquid. The former being more anharmonic than the latter, one should expect a smaller frequency variation of the viscosity $D_T''(\omega)$ of a hard-sphere fluid compared with that one of

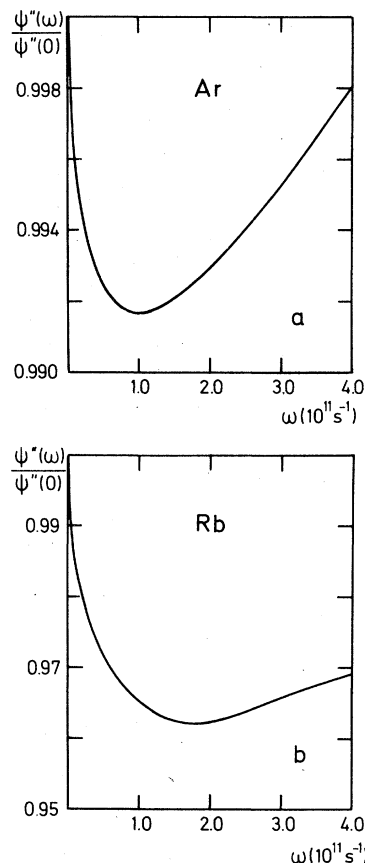


FIG. 2. Low-frequency velocity-autocorrelation spectra of Ar (a) and Rb (b).

Ar or Rb. It is worthwhile mentioning that, although the asymptotic tail (2) can be explained with simple phenomenological scaling arguments, it requires a microscopic theory to understand why the range of validity of the asymptote is so small.

Some final comments on the numbers presented in Figs. 1 and 2 and Table I should be made. The full curves of Fig. 1 were calculated with the same data as in Ref. 15. Hence they can be thought of as a continuation of the curves of Fig. 2 of Ref. 15 to smaller frequencies, since the contribution¹⁵ from nonhydrodynamic modes, $M_{BGZ}''(\omega)$, where $M_{BGZ}''(\omega)$ denotes relaxation spectrum in Bosse, Götze, and Zippelius paper (Ref. 15), can be taken to be constant over the frequency range $\omega < 4 \times 10^{11} \text{ s}^{-1}$ discussed here. That has been done in order to calculate

$$M''(\omega) = M''(\omega)^H + M_{BGZ}''(\omega)$$

in Fig. 1 and with it $\psi''(\omega)/\psi''(0)$ in Fig. 2.

Since the repulsive part of the Rb potential is softer than that of Ar, one expects the "viscoelastic" effect ($\delta_T < 1$) of a frequency-dependent viscos-

ity which weakens the long-time tail to be stronger in Rb than in Ar. That is indeed confirmed by the difference between the dash-dotted curve ($\delta_T=1$) and the full curve ($\delta_T < 1$) being larger in Rb than in Ar. Nevertheless, the Rb long-time tail remains stronger with our parameters (Table I) than that one of Ar as a consequence of the larger square-root steepness ω_0^{-1} [Eq. (5)] entering Eq. (6). The spectra $M''(\omega)$ and $\psi''(\omega)$ and consequently also the tail strength σ do, however, depend on the size of the transport coefficients like D_T , for example. We used the values of Table I which were

determined in the earlier theory^{14,15} and which differ from the experimental ones¹⁷ by factors up to 2 or 3 in the case of Ar. If for Ar one used the data of Levesque *et al.*¹⁶ as input for δ_T , Γ_T , and D_T , the Ar long-time spike in Fig. 2 would have a strength of $\sigma \approx 0.05$. Thus a quantitative evaluation of the long-time tail strength σ all within the mode-coupling theory¹³⁻¹⁵ is somewhat obliterated by the uncertainties of the transport coefficients. However, we believe that the physics of the suppression of the long-time anomaly is explained correctly by the analysis presented here.

¹For a review up to 1975, see Y. Pomeau and P. Resibois, *Phys. Rep.* **19**, 64 (1975).

²B. J. Alder and T. Wainwright, *Phys. Rev. Lett.* **18**, 988 (1967).

³B. J. Alder and T. Wainwright, *Phys. Rev. A* **1**, 18 (1970).

⁴R. Zwanzig and M. Bixon, *Phys. Rev. A* **2**, 2005 (1970).

⁵J. Dorfman and E. Cohen, *Phys. Rev. Lett.* **25**, 1257 (1970); *Phys. Rev. A* **6**, 776 (1972).

⁶B. J. Berne, J. P. Boon, and S. A. Rice, *J. Chem. Phys.* **45**, 1086 (1966).

⁷A. Rahman, *Phys. Rev.* **136**, A405 (1964).

⁸D. Levesque and W. T. Ashurst, *Phys. Rev. Lett.* **33**, 277 (1974).

⁹P. Michels and N. J. Trappeniers, *Physica A* **90**, 179

(1978).

¹⁰P. A. Egelstaff, *An Introduction to the Liquid State* (Academic, London, 1967).

¹¹K. Carneiro, *Phys. Rev. A* **14**, 517 (1976).

¹²K. Sköld, J. M. Rowe, G. Ostrowski, and P. D. Randolph, *Phys. Rev. A* **6**, 1107 (1972).

¹³J. Bosse, W. Götze, and M. Lücke, *Phys. Rev. A* **17**, 434 (1978).

¹⁴J. Bosse, W. Götze, and M. Lücke, *Phys. Rev. A* **17**, 447 (1978); **18**, 1176 (1978).

¹⁵J. Bosse, W. Götze, and A. Zippelius, *Phys. Rev. A* **18**, 1214 (1978).

¹⁶D. Levesque, L. Verlet, and J. Kurkijärvi, *Phys. Rev. A* **7**, 1690 (1973).

¹⁷D. G. Naugle, J. H. Lunsford, and J. R. Singer, *J. Chem. Phys.* **45**, 4669 (1966).